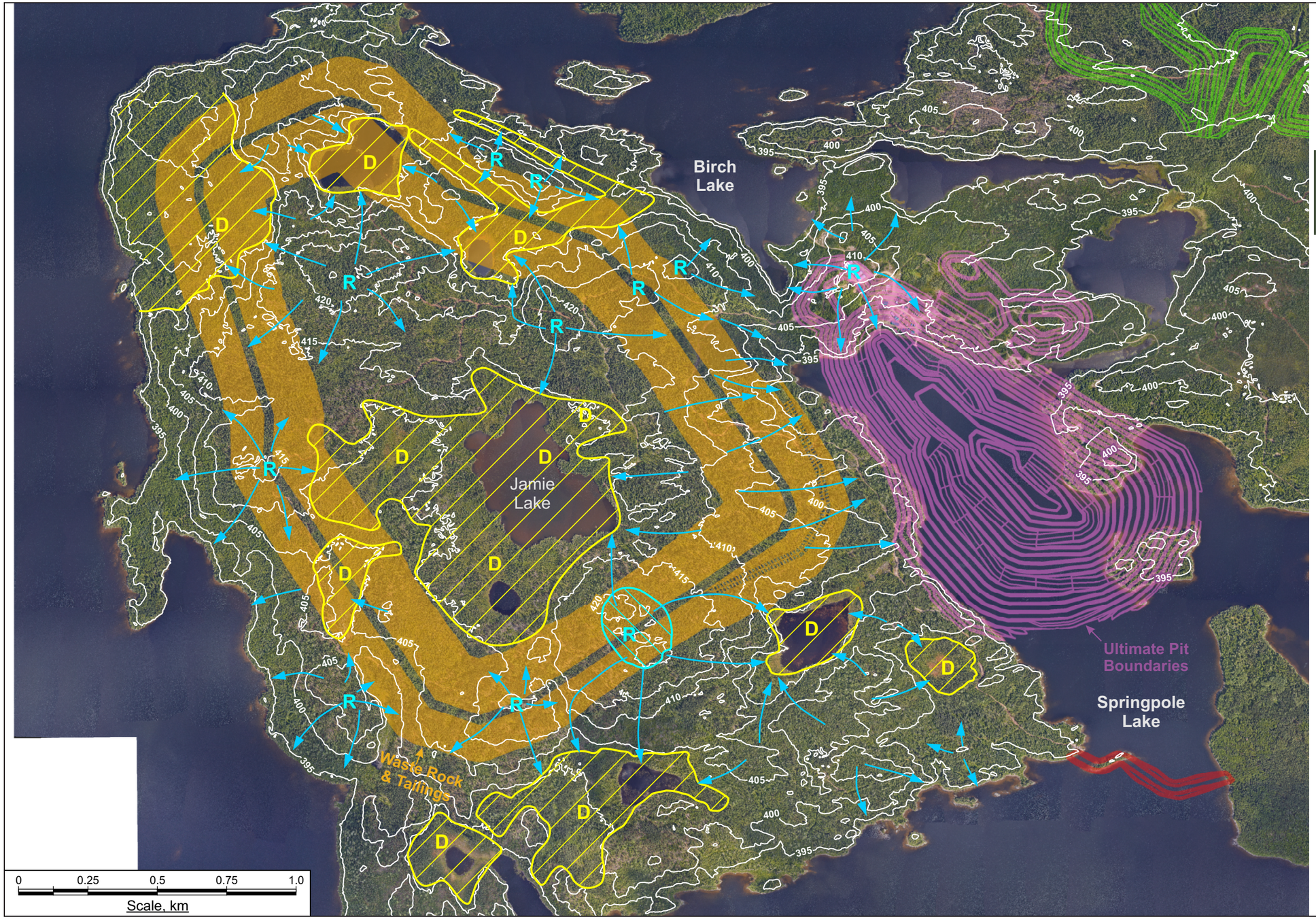

N

Legend

- R — Recharge area
- D — Discharge area
- Inferred flow direction
- 405 — Elevation contours in metre

Note

1. Contour map provided by First Mining Gold Corp, 2019
2. Base orthorectified image provided by First Mining Gold Corp, 2020.
3. Infrastructure map provided by First Mining Gold Corp, 2021.

Figure 1.3

Contour map from Lidar data showing local groundwater recharge (R) and discharge (D) areas with flow lines and perimeter of proposed waste rock storage area.

Project No.	3134
Location	Springpole, ON
Document Reference	FFC-NL-3134-002
Date	March 2021

FFC

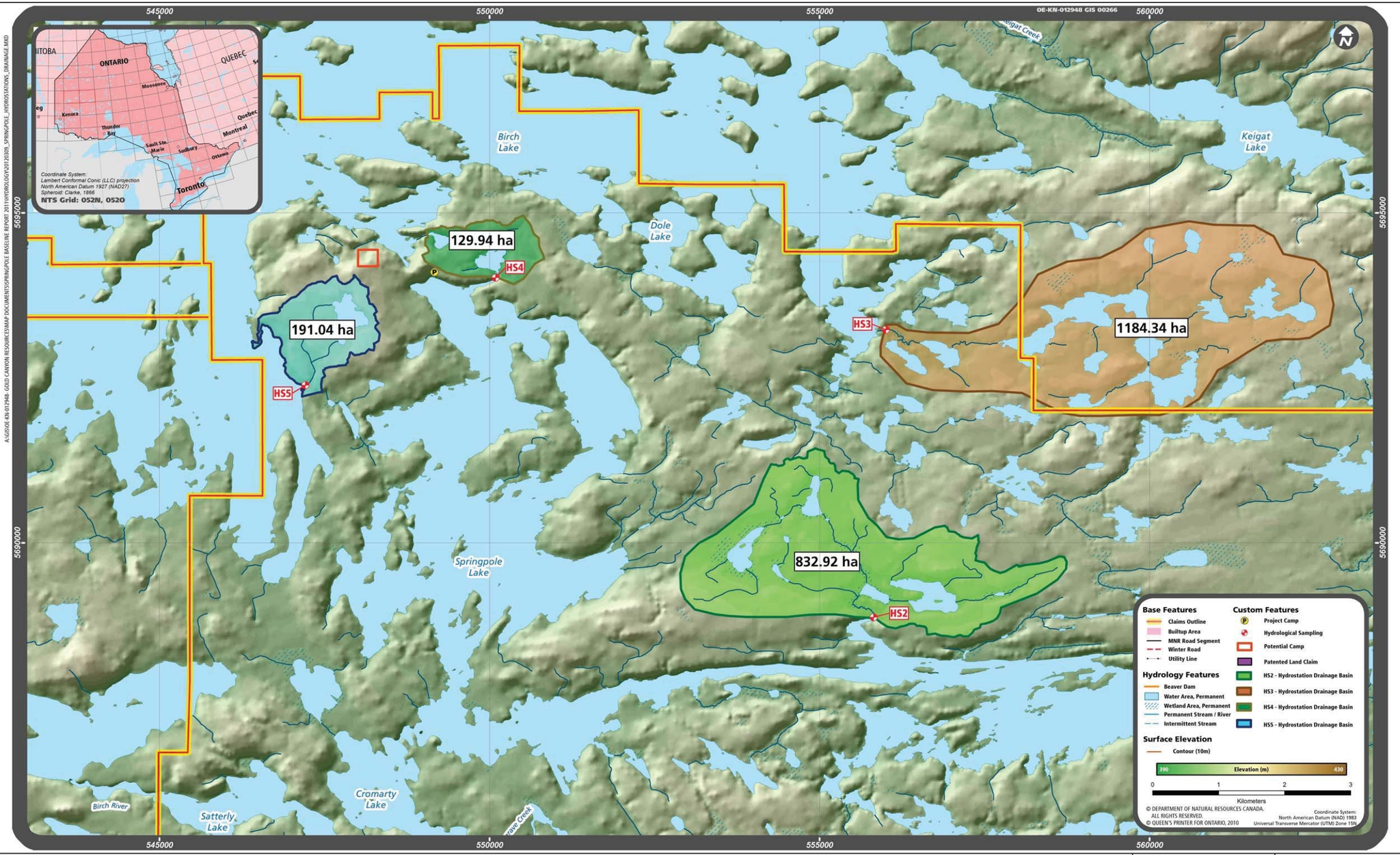

Figure 1.4 Outline of four main drainage basins (After DST). Base map provided by First Mining Gold.

Project No.	Document Reference
3134	FFC-NL-3134-002
Location	Date
Springpole, ON	December 2019

FFC

2.0 OVERBURDEN AND SHALLOW BEDROCK GROUNDWATER FLOW SYSTEM

2.1 Geotechnical Program

The geology and hydrogeology of the overburden and shallow fractured bedrock was investigated in 2020, using geotechnical boreholes, test pits, drive points and GPR surveys followed by laboratory analysis of the collected rock and soil samples (Fracflow, 2020a). The main project components that were the focus of this program include the proposed mine rock storage area (WSF1), Plant Site area (PS), and the original Stockpile area (SP) which is located on the east side of the open pit, and the proposed mine rock storage area (WSF2) which is located on the west side of open pit and includes the proposed Tailings Management Facility area (TMF). The Stockpile area has been relocated to the WSF1 area, east of the starter pit. The geotechnical field program consisted of drilling and sampling 14 geotechnical boreholes (all drilled during the summer 2020 program), and investigation of overburden at 32 locations using test pit excavation (21 locations), hand augering (9 locations), and diamond drilling in lieu of test pit excavation (2 locations) (**Figure 2.1**).

The standard operating procedures utilized in the geotechnical test pit excavation and hand augering consisted of soil profile identification, hand held penetrometer test in test pits only, micro-shear vane test in test pits only, and soil sampling followed by laboratory tests (grain size analysis, including hydrometer tests, Proctor Tests, and Atterberg Limits tests on selected soil samples). Additional laboratory tests were completed on selected overburden samples by other consultants and are not provided in this report. The geotechnical boreholes were completed using a NW/NQ diamond drill string to conduct standard penetration tests (SPTs), dynamic cone penetration tests (DCPTs), field shear vane test, and to collect soil samples using split spoon samplers and Shelby tubes. All of the geotechnical boreholes were extended from 2 m to 10 m into the shallow bedrock.

Piezometers were installed in the geotechnical boreholes, with one piezometer interval located in the fractured bedrock and one piezometer interval located in the granular overburden, where the thickness of the overburden permitted. Bentonite seals were used to isolate each piezometer interval to provide a measure of vertical hydraulic gradients as well as an accurate measure of the water table elevation. Measurement of the water table elevations in adjacent boreholes confirmed the recharge and discharge conditions between the elevated areas and the adjacent depressions. Falling head tests were completed in each piezometer and test pit standpipe to determine the hydraulic conductivity of the subsurface material. The detailed logs for the boreholes, test pits and hand augered holes along with the relevant field and laboratory data are provided in the geotechnical factual report (Fracflow, 2020a).

Figure 2.2 shows the location of the five auger holes and five drive points that were advanced in 2019 at different locations in the original Tailings Management Area (TMA) (**Appendix A**), which is located approximately 5 km southeast of the proposed open pit. The auger holes were

advanced using a hand-operated open-head auger unit which provided samples of the underlying material. The bog or peat layer thickness ranged from 2.64 m to 8.5 m. Close to the west end of the central lake, at the lake shoreline, the bog or peat layer (G002) appeared to be floating. The fine to medium sand layer below the peat layer was dense and difficult to penetrate. Refusal on rock was obtained at approximately 9.5 m of depth at this hand auger location. The one-inch (25.4 mm) stainless steel drive points were advanced using an electric jack-hammer to refusal on rock or very dense sand. The low water levels in the drive points are assumed to reflect time-lag in the piezometers due to low permeability of the surrounding overburden. The field data, detailed logs and GPR profiles for this area are provided in **Appendix A**.

2.2 Overburden Geology

For convenience in discussing the geology and hydrogeology of the overburden, the Springpole Lake Project site has been divided into three sub-areas: (1) The eastern site, (2) the western site, and (3) the plant site.

Test Pits

Eastern Site: Overburden in the area of test pit TP-WSF1-02 and TP-WSF1-03 (**Figure 2.1**) can be described as a layer of peat and organic material overlying a layer of sticky silty/clay layer, which overlies bedrock. Overburden in the area of test pits TP-WSF1-07 and TP-WSF1-08 can be described as layers of sandy silt with trace gravel and trace clay, which overlie bedrock. Overburden in the area of test pits TP-WSF1-04, TP-WSF1-05, TP-WSF1-23, and TP-WSF1-32 can be described as a layer of peat and organic material overlying a layer of sticky silt/clay layer followed by a sandy layer, which overlies bedrock. Overburden in the area of test pits TP-WSF1-06 and TP-WSF1-22B can be described as a shallow layer of sand and silt with gravel, which overlies bedrock.

Western Site: Overburden in the area of test pit TP-TMF-11C (**Figure 2.1**) can be described as a layer of peat and organic material overlying a shallow sand layer, which overlies bedrock. Overburden in the area of test pits TP-TMF-12, TP-TMF-13 and TP-TMF-14 can be described as a thick sandy layer followed by a silt/clay layer, which overlies bedrock. Overburden in the area of test pits TP-TMF-12, TP-TMF-15, and TP-TMF-16 can be described as a thick layer of sand, with cobbles and boulders, some gravel, and trace clay, which overlies bedrock. Overburden in the area of test pits TP-WSF2-09 and TP-WSF2-09B can be described as a layer of peat and organic material overlying a sandy layer followed by a clay layer, which overlies bedrock. Overburden in the area of test pits TP-WSF2-24A and TP-WSF2-25A can be described as a thick layer of dark brown soil that overlies a clay layer, which overlies bedrock. Overburden in the area of test pit TP-WSF2-26 can be described as a layer of peat and organic matter overlying silty gravelly sand, with trace clay, which overlie bedrock.

Plant Site: Overburden in the area of test pits TP-PS-18 and TP-PS-19 can be described as a thick layer of silty sand, with some gravels, cobbles and boulders, and trace clay, which overlies bedrock. Overburden in the area of test pits TP-SP-17, TP-SP-20, and TP-SP-21 can be described as a layer of silt/clay with trace sand and gravel that overlies sandy layers, with trace silt/clay and gravel, which overlie bedrock. Overburden in the area of test pits TP-PS-28, TP-PS-29, TP-PS-30D and TP-PS-31 can be described as a peat and organic material layer overlying a clay layer, followed by a fine sand layer, which overlies bedrock.

Overburden thickness in the test pits ranged from 0.31 m in TP-WSF1-06A to 4.95 m in TP-WSF2-24A. The fine grained silty clay or clayely silt layers that are present in some of the western areas were deposited in quiet lagoonal (glacial fluvial) environments and are primarily restricted to depressions. The granular layers with cobbles are primarily till. However, in some areas, such as the proposed plant site, the distinct sand and gravel layers did indicate that they were water laid.

Boreholes

Eastern Site: Overburden in the area of boreholes BH-WSF1-01 and BH-WSF1-12 can be described as a layer of peat followed by a sand/silt layer overlying a silt/clay layer, which overlies bedrock. Overburden in the area of boreholes BH-WSF1-02 and BH-WSF1-03 can be described as a layer of peat and organic material overlying a silt/clay and some sand layer, which overlies bedrock. Overburden in the area of borehole BH-WSF1-11 can be described as a layer of peat and organic material overlying a sticky silt/clay layer followed by a sandy layer with gravel, which overlies bedrock.

Western Site: Overburden in the area of boreholes BH-TMF-04 and BH-TMF-05 can be described as a layer of fine sand and silt with gravels overlying bedrock. Overburden in the area of borehole BH-TMF-15 can be described as a layer of peat and organic material overlying sticky silt/clay layer followed by a layer of silt and some sand, which overlies bedrock. There was no recovery to describe the overburden in the area of borehole BH-WSF2-06. Overburden in the area of borehole BH-WSF2-13 can be described as a silty clay layer with some sand followed by a coarse sand layer, which overlies bedrock. Overburden in the area of borehole BH-WSF2-14 can be described as a layer of sand with fines, which overlies bedrock.

Plant Site: Overburden in the area of borehole BH-PS-07-R1, BH-PS-08-R1, and BH-PS-09-R1 can be described as a layer of peat and organic material overlying a silt/sand layer with some clay and gravel, which overlies bedrock.

Overburden thickness in the boreholes ranged from 1.22 m in BH-PS-07-R1 to 5.78 m in BH-TMF-15. In BH-TMF-15, a silty clay layer, approximately 3 m thick, was encountered at 393.3 m elevation. Since the fine grained silty-clay material was most likely deposited in a quiet lagoon setting or an impounded glacial melt-water lake, this elevation provides a useful reference

for determining the extent of a silty-clay layer in individual depressions or low lying areas. However, it is expected that the elevation and thickness of the silty-clay layers will vary, depending on the extent to which the local depressions are connected.

2.3 Hydraulic Conductivity Values for Overburden and Shallow Bedrock

The hydraulic conductivity values for the overburden and shallow bedrock were estimated by applying the Hazen Method to the grain size distribution data for the granular overburden samples (Fetter, 2001) and by conducting falling head or rising head tests on the piezometers in the geotechnical boreholes and standpipes in the test pits. The laboratory and field procedures and data on which those hydraulic conductivity values were computed are tabulated in the geotechnical factual report (Fracflow, 2020a).

Applying the Hazen method to the selected samples provided hydraulic conductivities (**Table 2.1**) that ranged from 1.67 E-09 m/s to 1.76 E-04 m/s for the overburden samples that were analyzed. The grain sizes of the fine-grained soil samples in this suite of soil samples fall below the range in which the Hazen method applies.Therefore, the conductivity values calculated here for those samples represent an estimate or approximation to the in-situ hydraulic conductivity values. **Figure 2.3** provides the hydraulic conductivity values in the form of a cumulative probability plot, which provides a measure of the mean (3.26 E-07 m/s) and standard deviation (9.10 E-06 m/s) for the overburden data derived from laboratory tests.

Falling head tests were completed in 12 boreholes and 21 test pits and the estimated hydraulic conductivity (K) of the subsurface materials around each well screen was determined using the method of Bouwer and Rice (Bouwer, 1989). The K values that were obtained from the falling head tests in standpipes and piezometers are provided in **Table 2.2** and **Table 2.3**. The in-situ hydraulic conductivity values for the overburden test intervals and the shallow bedrock test intervals are presented as cumulative probability plots (**Figures 2.4 and 2.5**). The hydraulic conductivity values of the in-situ overburden piezometer intervals had a range of 3.64 E-06 m/s to 7.61 E-04 m/s with a mean of 3.75 E-05 m/s and a standard deviation of 1.55 E-04 m/s. The in-situ shallow bedrock piezometer intervals had a hydraulic conductivity range of 2.84 E-07 m/s to 3.08 E-05 m/s with a mean of 4.17 E-06 m/s and a standard deviation of 1.24 E-05 m/s.

2.4 Bedrock and Silty Clay Zones from Ground Penetrating Radar (GPR) Profiles

In 2019 and 2020 program, GPR surveys were conducted along the south edge and the north-eastern edge of the proposed Mine Rock and Tailings storage area using either a dual frequency GPR antenna or a single frequency antennae to map depths to bedrock and to locate possible clay zones. **Figures 2.6a, 2.6b** and **2.6c** show the location of the GPR survey lines that were completed in the proposed Mine Rock and Tailings storage area and the immediate north end of

the proposed open pit. The full suite of GPR images and profiles are provided in Fracflow (2020a) and **Appendix C**.

The depth to bedrock has been interpreted using test pit data, borehole data and DCPT data. Those reference points, test pits, DCPTs and boreholes are shown on the relevant images or profiles. Clay layers or layers that are rich in clay tend to smear the GPR image and a number of the large clay layers are outlined on the GPR images or profiles. In addition, a GPR survey was conducted across what was expected to be a thicker overburden section between Birch Lake and Springpole Lake, confirming the presence of the thicker overburden in that area (**Appendix C**).

Comparison of the GPR profiles with the Lidar map shows that the depressions generally have fine-grained soils to some extent and that the high ground is generally areas with thin overburden, primarily organics and granular materials, or exposed bedrock. The GPR profiles (Fracflow, 2020a) also show a number of near vertical smeared or high conductivity zones that extend to depth. Those zones are interpreted as bedrock structures such as shear zones that contain fine grained gouge material.

2.5 Hydrogeology of the Overburden and Shallow Bedrock System

Overall, all areas of the project site have very low relief with the difference in elevation of the landmass that is located between Springpole Lake and Birch Lake not exceeding 25 to 30 m. The project site area is characterized by a series of rolling hills with intervening depressions. The depressions have relatively thick overburden up to at least 5 m thick and the overburden on the high ground generally ranges from exposed bedrock to a metre or so of organic and granular cover. The water table is close to the surface in the depressions but can be up to 2.6 m or more below ground surface on the high ground. **Table 2.4** and **Table 2.5** provide the water level elevations that have been calculated based on the survey elevation data for each monitoring well and each test pit standpipe that were provided by Stantec Engineering. The small number of water level data points, relative to the rapid changes in topography, does not permit the contouring of a water table map. However, the water table measurements are essential to calibration of a 3D numerical flow and transport model where the topographic detail can be included in the model mesh.

The overburden in the plant site area is generally thicker than the average overburden thickness in both the western and eastern areas of the site, except for the area between the northern end of Springpole Lake (the camp zone) and Birch Lake. The overburden column in the proposed plant site is similar to that which was mapped in the original TMA area, approximately 5 km to the southeast.

Near surface fractured bedrock normally has a porosity of less than 1% while overburden materials generally have porosities that range from 20% to 40% or more. However, fractured bedrock has a wide range of hydraulic conductivity values when compared to a typical layer of

granular overburden and the regularly-fractured bedrock normally exhibits a logarithmic decrease in permeability with depth below the ground surface.

Based on the low relief within and around the Springpole Lake Project site, and the number of small hills and adjacent depressions (**Figure 1.4**), the shallow groundwater flow system is characterized by a number of small recharge areas (the elevated areas) and adjacent discharge areas (the adjacent depressions) producing a shallow to intermediate groundwater flow system that interacts with the small surface water drainage basins and the larger lakes. The small streams tend to respond rapidly to rainfall events with a rapid decrease in stream flow at the end of the rainfall event indicating limited baseflow. This is consistent with the observations of overland and interflow during intense rainfall events.

Recharge to the deeper groundwater flow system is considered to be limited. The deeper groundwater flow system is considered to be relatively stagnant with low groundwater gradients (estimated at <0.0001) and low groundwater velocities (estimated at < 0.00001 m/day) that are typical of low permeability regional bedrock flow systems. Excavation and dewatering of the proposed open pit will have a significant but temporary impact on both the shallow and the deep groundwater flow system baseline conditions but with the deep flow system being re-established as the pit lake is flooded at the end of mining.

2.6 Role of Lake Sediments in Controlling Shallow Flow System Recharge

The surface of Jamie Lake (**Figure 2.7**) is elevated with respect to Springpole Lake and Birch Lake. A GPR survey was conducted along a number of transects to obtain images of the lake bottom. **Figure 2.8** shows a typical lake bottom GPR image for Jamie Lake that shows the small boulders or cobbles along with lake-bottom sediments. The soft sediments create a low permeability layer on the bottom of the lake that impedes recharge to the underlying fractured bedrock and is expected to reduce the impacts of the overall open pit dewatering on Jamie Lake. However, Jamie Lake is expected to be filled with tailings and the lake sediments will impede pore fluids that originate in the tailings from migrating into the underlying fractured bedrock. Collection of piston cores from the lake ice cover can confirm the presence and permeability characteristics of the lake bottom sediments. The full suite of lake bottom GPR images are presented in Fracflow (2020b).

Table 2.1 Hydraulic conductivity calculated using the Hazen method.

Sample ID	Effective Grain Size (d_{10}) (cm)	Coefficient (C)	Hydraulic Conductivity (K) (cm/s)
Eastern Site			
TP-WSF1-04-SS2	1.40 E-04	40	7.84 E-07
TP-WSF1-05-SS2	1.20 E-04	50	7.20 E-07
TP-WSF1-07-SS1	7.00 E-04	60	2.94 E-05
TP-WSF1-07-SS2	2.20 E-03	60	2.90 E-04
TP-WSF1-07-SS3	1.50 E-03	60	1.35 E-04
TP-WSF1-08-SS1	7.60 E-04	50	2.89 E-05
TP-WSF1-08-SS2	2.37 E-03	50	2.81 E-04
Western Site			
TP-WSF2-09-SS1	5.00 E-04	90	2.25 E-05
TP-WSF2-09-SS2	5.80 E-05	50	1.68 E-07
TP-WSF2-09B-SS1	9.50 E-04	80	7.22 E-05
TP-WSF2-09B-SS2	7.10 E-04	80	4.03 E-05
TP-TMF-12-SS1	1.85 E-03	70	2.40 E-04
TP-TMF-13-SS2	5.90 E-04	80	2.78 E-05
TP-TMF-13-SS5	8.00 E-04	90	5.76 E-05
TP-TMF-15-SS1	1.10 E-03	60	7.26 E-05
TP-TMF-16-SS1	2.45 E-04	90	5.40 E-06
TP-TMF-16-SS2	1.60 E-04	50	1.28 E-06
TP-TMF-16-SS3	1.00 E-03	50	5.00 E-05
TP-WSF2-23A-SS2	9.50 E-05	40	3.61 E-07
TP-WSF2-26-SS1	1.71 E-03	70	2.05 E-04
BR-005-SS1	1.80 E-04	40	1.30 E-06
Plant Site			
TP-SP-17-SS2	9.00 E-05	40	3.24 E-07
TP-SP-17-SS3	1.10 E-03	40	4.84 E-05
TP-SP-17-SS4	5.20 E-03	60	1.62 E-03
TP-SP-17-SS5	1.40 E-02	90	1.76 E-02
TP-PS-18-SS1	6.50 E-03	90	3.80 E-03
TP-PS-19-SS1	1.10 E-03	40	4.84 E-05
TP-PS-20-SS2	1.30 E-03	40	6.76 E-05
TP-PS-20-SS4	1.20 E-02	90	1.30 E-02
TP-PS-20-SS5	4.40 E-03	50	9.68 E-04
TP-PS-20-SS6	1.19 E-03	50	7.08 E-05
TP-PS-21-SS3	9.50 E-04	40	3.61 E-05
TP-PS-21-SS4	1.10 E-03	50	6.05 E-05
TP-PS-31-SS1	1.80 E-04	90	2.92 E-06
TP-PS-31-SS2	7.50 E-05	50	2.81 E-07

Table 2.2 Hydraulic conductivity calculated using the standpipe in the test pits to conduct falling head test.

Test Pit ID	Hydraulic Conductivity (m/s)	Test Interval Material Type
Eastern Site		
TP-WSF1-02A	3.04E-04	Overburden (Black soil and organic material)
TP-WSF1-04	6.51E-05	Overburden (Clay layer which overlies sand and gravel layer)
TP-WSF1-05	2.01E-05	Overburden (Clay layer which overlies sand layer)
TP-WSF1-07	8.08E-06	Overburden (Silt and fine sand)
TP-WSF1-23A-Deep	1.20E-05	Overburden (Clay layer which overlies sand and silt layer)
Western Site		
TP-TMF-10	3.64E-06	Overburden (silt and gravel) and fractured bedrock
TP-TMF-12	7.61E-04	Overburden (Sand and gravel)
TP-TMF-13	1.02E-05	Overburden (Sand layer which overlies silt/clay layer)
TP-TMF-15	2.03E-04	Overburden (Sand and gravel)
TP-WSF2-26	3.07E-04	Overburden (Peat layer which overlies sand layer)
TP-TMF-27	8.66E-06	Fractured bedrock
TP-TMF-14	4.19E-05	Overburden (Sandy silt layer which overlies clay and gravel)
TP-WSF2-24A	9.88E-06	Overburden (Clay)
TP-WSF2-25A	3.27E-05	Overburden (Clay layer which overlies sand layer)
Plant Site		
TP-SP-17	3.05E-05	Overburden (Silt/clay layer which overlies sand layer)
TP-PS-18	2.58E-05	Overburden (Silty/clayey sand, cobbles and boulders)
TP-PS-19	6.02E-05	Overburden (Silty sand, cobbles and boulders)
TP-PS-20	1.41E-05	Overburden (Sand and silt)
TP-PS-21	4.09E-05	Overburden (Clay layer which overlies sand and silt layer)
TP-PS-28	6.62E-05	Overburden (Silt/clay layer which overlies sand layer)
TP-PS-29	1.04E-04	Overburden (Peat, organic material)

Table 2.3 Hydraulic conductivity calculated using the piezometer in the boreholes to conduct falling head test.

Borehole ID	Hydraulic Conductivity (m/s)	Test Interval Material Type
Eastern Site		
BH-WSF1-02-Deep	1.39E-06	Fractured bedrock
BH-WSF1-02-Shallow	2.87E-06	Overburden (Silt/clay and silty/clayey sand)
BH-WSF1-03-Deep	2.84E-07	Fractured bedrock
BH-WSF1-03-Shallow	1.37E-05	Fractured bedrock
BH-WSF1-11-Deep	2.58E-05	Fractured bedrock
BH-WSF1-11-Shallow	3.30E-06	Overburden (Peat layer which overlies clay layer)
BH-WSF1-12-Deep	3.30E-06	Fractured bedrock
BH-WSF1-12-Shallow	2.09E-05	Overburden (Silt/clay and sand) and fractured bedrock
Western Site		
BH-TMF-04-Deep	3.85E-07	Fractured bedrock
BH-TMF-04-Shallow	2.36E-06	Fractured bedrock
BH-TMF-05	2.75E-06	Fractured bedrock
BH-WSF2-13-Deep	2.03E-06	Fractured bedrock
BH-WSF2-13-Shallow	2.05E-06	Overburden (Sand) and fractured bedrock
BH-WSF2-14-Deep	1.28E-06	Fractured bedrock
BH-WSF2-14-Shallow	3.96E-06	Fractured bedrock
BH-TMF-15-Deep	2.48E-06	Fractured bedrock
BH-TMF-15-Shallow	1.73E-06	Overburden (Silt/clay)
Plant Site		
BH-PS-07-R1-Deep	1.69E-06	Fractured bedrock
BH-PS-07-R1-Shallow	8.45E-06	Fractured bedrock
BH-PS-08-R1-Deep	8.52E-06	Fractured bedrock
BH-PS-08-R1-Shallow	1.18E-05	Overburden (Clay and sand) and fractured bedrock
BH-PS-09-R1-Deep	1.55E-05	Fractured bedrock
BH-PS-09-R1-Shallow	3.09E-05	Overburden (Sand) and fractured bedrock

Table 2.4 Water level elevations calculated for geotechnical test pits.

Test Pit ID	Ground Surface			Top of Riser Elevation (m)	Date (dd/mm/yy)	Water Depth (m bgs)	Water Elevation (m)
	UTM (NAD 83-15)		Elevation (m)				
	Easting	Northing					
Eastern Site							
TP-WSF1-02A	549843.0	5695400.2	395.72	396.97	06/09/20	0.201	395.577
TP-WSF1-03D	549830.5	5694927.0	402.39	404.24	06/09/20	0.068	402.33
TP-WSF1-04	550085.5	5694972.1	398.95	400.48	06/09/20	0.078	398.923
TP-WSF1-05	550740.9	5694797.9	400.32	401.99	05/09/20	0.461	399.918
TP-WSF1-06A	551278.5	5694859.8	400.30	401.25	NA	NA	NA
TP-WSF1-07	550395.2	5694180.7	407.33	406.95	04/09/20	Dry	NA
TP-WSF1-08	550925.6	5694246.0	409.13	410.23	05/09/20	0.118	409.126
TP-WSF1-23A-Deep	550440.43	5694548.04	399.94	402.11	08/09/20	0.409	399.531
TP-WSF1-23A-Shallow				402.07	08/09/20	0.329	399.611
Western Site							
TP-WSF2-09	547297.0	5694422.2	414.04	413.87	07/09/20	0.004	411.983
TP-TMF-10	546925.0	5693579.5	414.68	414.84	06/09/20	0.092	414.57
TP-TMF-12	548427.7	5693763.4	409.31	410.77	07/09/20	0.000	409.334
TP-TMF-13	548170.8	5693400.9	411.17	412.44	07/09/20	0.227	410.996
TP-TMF-14	547534.3	5692622.0	405.92	407.41	06/09/20	0.553	405.184
TP-TMF-15	549165.0	5692963.7	404.87	406.02	08/09/20	0.594	404.4
TP-TMF-16	548423.7	5692282.7	403.48	405.02	08/09/20	1.927	401.991
TP-WSF2-24A	547406.7	5694738.3	397.72	398.56	07/09/20	0.275	397.462
TP-WSF2-25A	546904.4	5694579.8	403.08	405.04	07/09/20	0.145	402.993
TP-WSF2-26	548915.4	5692433.6	404.06	405.83	08/09/20	0.040	404.19
TP-TMF-27	547099.5	5693190.2	404.27	404.42	06/09/20	0.078	404.219
TP-WSF1-32	549748.3	5695043.8	400.64	401.87	06/09/20	0.138	400.769
Plant Site							
TP-SP-17	550371.6	5693641.2	392.92	394.32	04/09/20	1.619	391.556
TP-PS-18	550092.1	5693759.1	396.93	398.52	04/09/20	Dry	NA
TP-PS-19	550200.0	5693852.3	399.76	400.84	04/09/20	Dry	NA
TP-PS-20	550527.5	5693625.7	396.47	397.84	04/09/20	0.968	395.626
TP-PS-21	550529.2	5693579.0	396.30	397.75	04/09/20	1.150	395.466
TP-PS-28	550486.1	5693831.9	399.79	400.15	04/09/20	0.049	399.667
TP-PS-29	550670.2	5693930.1	400.80	401.30	04/09/20	0.127	400.728
TP-PS-31	NA	NA	NA	406.96	04/09/20	0.646	404.345

Note: bgs: Below ground surface

NA: Not available

Table 2.5 Water level elevations calculated for geotechnical boreholes.

Test Pit ID	Ground Surface			Top of Riser Elevation (m)	Date (dd/mm/yy)	Water Depth (m bgs)	Water Elevation (m)
	UTM (NAD 83-15)		Elevation (m)				
	Easting	Northing					
Eastern Site							
BH-WSF1-01-Deep	549771.6	5695076.1	398.80	398.97	NA	NA	NA
BH-WSF1-01-Shallow				398.94	NA	NA	NA
BH-WSF1-02-Deep	550399.3	5694976.6	399.96	400.18	06/09/20	0.054	399.984
BH-WSF1-02-Shallow				400.20	06/09/20	0.128	399.906
BH-WSF1-03-Deep	550725.9	5694430.9	404.63	404.85	05/09/20	1.177	403.587
BH-WSF1-03-Shallow				404.86	05/09/20	0.357	404.399
BH-WSF1-11-Deep	551084.6	5694725.2	399.30	399.41	05/09/20	0.083	399.249
BH-WSF1-11-Shallow				399.43	05/09/20	0.082	399.245
BH-WSF1-12-Deep	549784.6	5695493.7	395.23	395.40	06/09/20	0.101	395.251
BH-WSF1-12-Shallow				395.40	06/09/20	0.005	395.344
Western Site							
BH-TMF-04-Deep	548122.1	5693470.9	412.57	413.66	07/09/20	1.457	411.095
BH-TMF-04-Shallow				413.70	07/09/20	1.489	411.063
BH-TMF-05	547428.0	5694197.7	413.31	413.62	07/09/20	0.222	413.142
BH-WSF2-06	548011.7	5694088.8	420.34	420.56	07/09/20	1.582	418.795
BH-WSF2-13-Deep	547290.0	5694515.2	401.47	401.89	07/09/20	0.529	401.03
BH-WSF2-13-Shallow				401.90	07/09/20	1.569	400.015
BH-WSF2-14-Deep	547152.3	5692979.7	404.20	404.55	06/09/20	0.300	403.995
BH-WSF2-14-Shallow				404.49	06/09/20	0.272	404.023
BH-TMF-15-Deep	549463.2	5692556.7	395.75	395.89	08/09/20	0.285	395.462
BH-TMF-15-Shallow				395.99	08/09/20	0.186	395.603
Plant Site							
BH-PS-07-R1-Deep	550473.5	5694183.5	404.85	405.11	04/09/20	2.561	402.372
BH-PS-07-R1-Shallow				405.09	04/09/20	0.729	404.208
BH-PS-08-R1-Deep	550666.2	5693923.4	400.80	400.97	04/09/20	0.520	400.341
BH-PS-08-R1-Shallow				400.95	04/09/20	0.390	400.472
BH-PS-09-R1-Deep	550747.0	5693840.8	400.40	400.76	05/09/20	0.430	400.104
BH-PS-09-R1-Shallow				400.74	05/09/20	0.393	400.134

Note: bgs: Below ground surface
NA: Not available

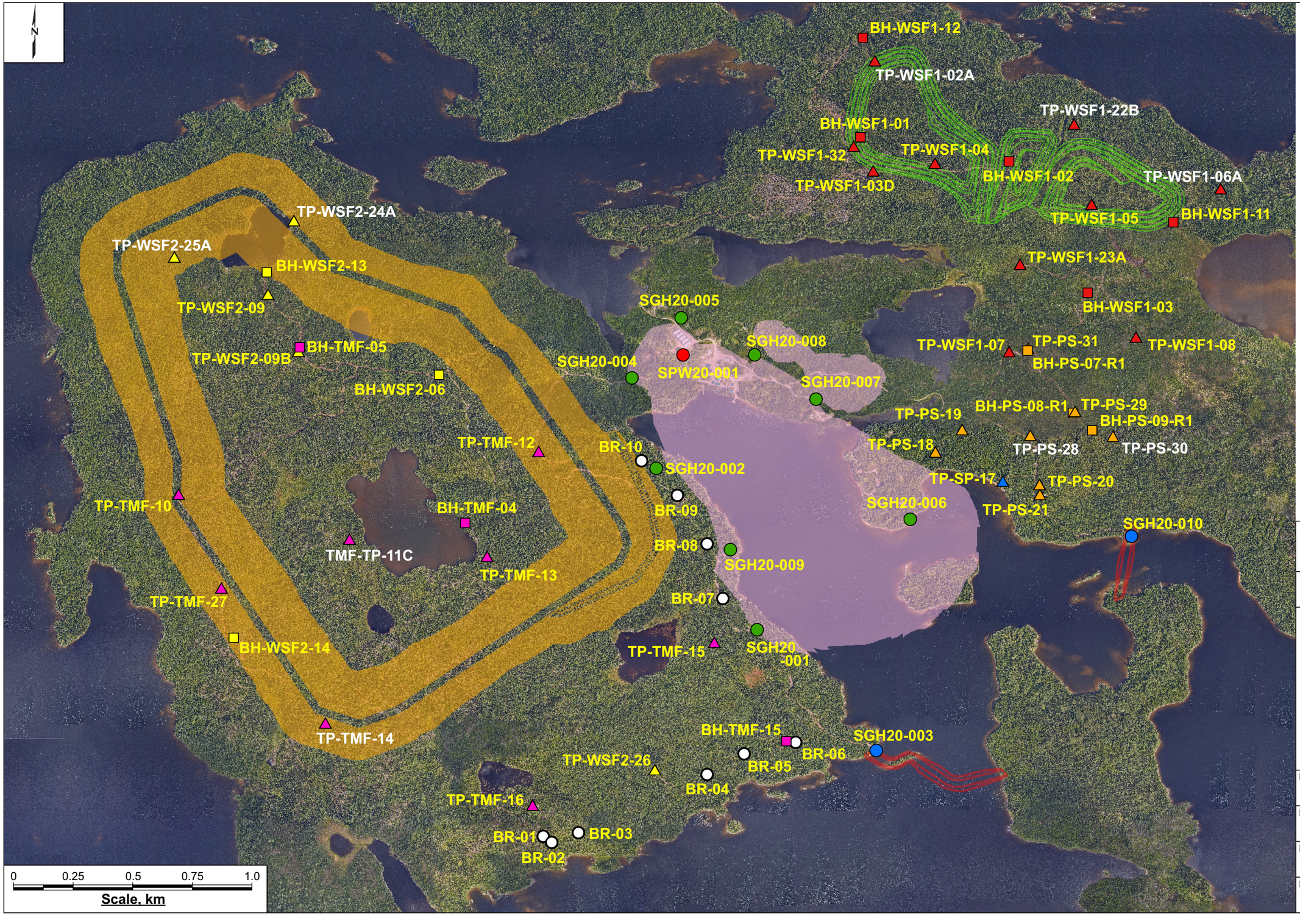

Legend

Geotech Borehole
- Plant Site
- Stockpile
- TMF
- WSF East
- WSF West

HydroGeo & Geotech
- Pit Slope Stability
- Coffer Dam

Test Pit
- Plant Site
- Stockpile
- TMF
- WSF East
- WSF West
- Bedrock Depth

Colour Legend for HoleID

BH-01	BH & TP Complete
TP-03	Hand Augerer - Complete

Base orthorectified image provided by First Mining Gold Corp.

Figure 2.1

Location map of completed boreholes and test pits for the winter-summer 2020 program at the Springpole site.

Project No.	3134
Location	Springpole, ON
Document Reference	FFC-NL-3134-002
Date	February 2021

FFC

Figure 2.2 Location of the five auger holes and five drive points advanced at different locations in the Tailings Management Area (TMA).

Project No.	Document Reference
3134	FFC-NL-3134-002
Location	Date
Springpole, ON	February 2021

FFC

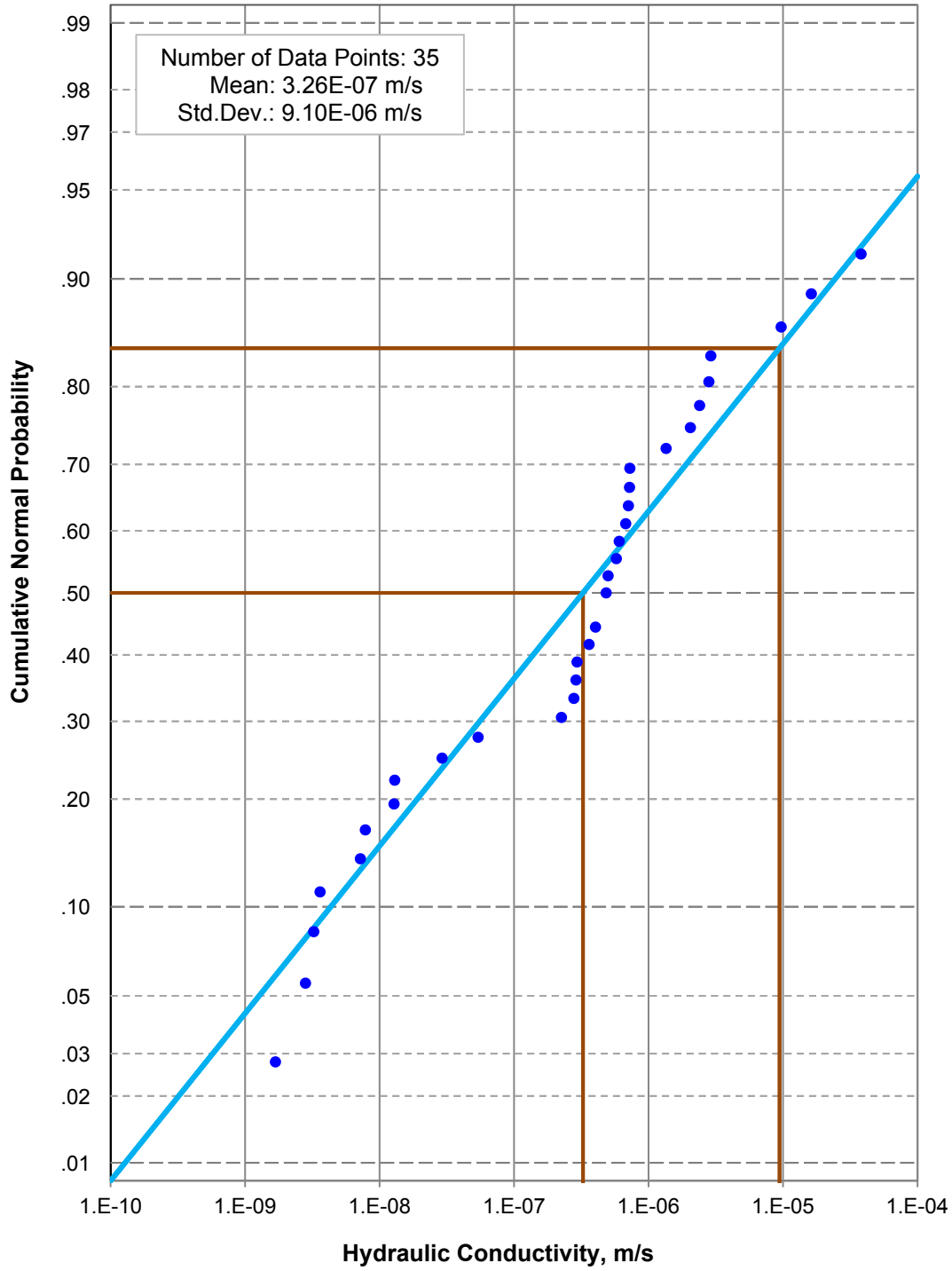

Figure 2.3 Cumulative normal probability plot of the hydraulic conductivities of test pits sample grain size analysis computed using the Hazen method.

Project No.	Document Reference
3134	FFC-NL-3134-002
Location	**Date**
Springpole, ON	February 2021

FFC

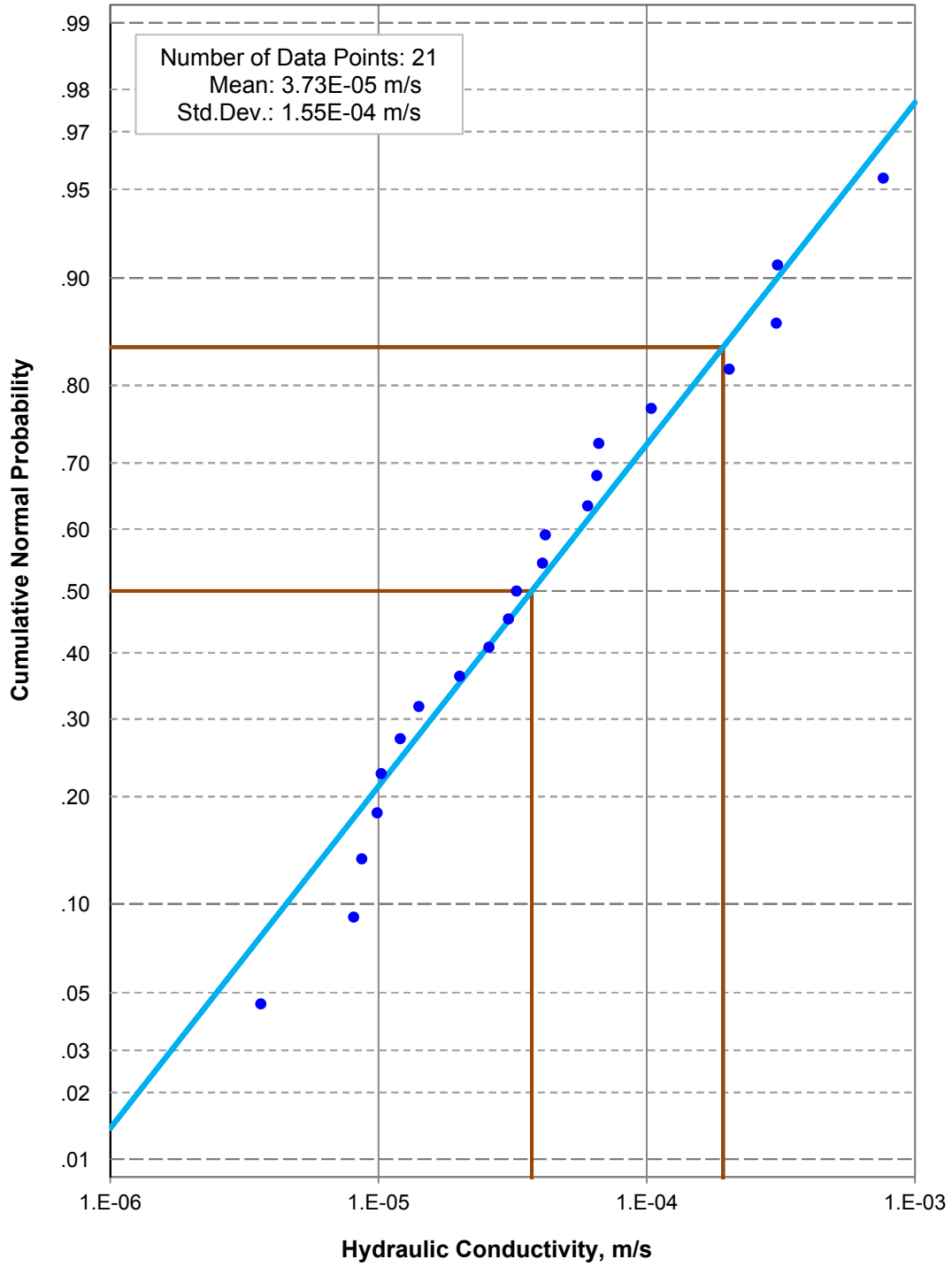

Figure 2.4 Cumulative normal probability plot of the hydraulic conductivities computed from falling head tests on test pit standpipes.

Project No.	Document Reference
3134	FFC-NL-3134-002
Location	Date
Springpole, ON	February 2021

FFC

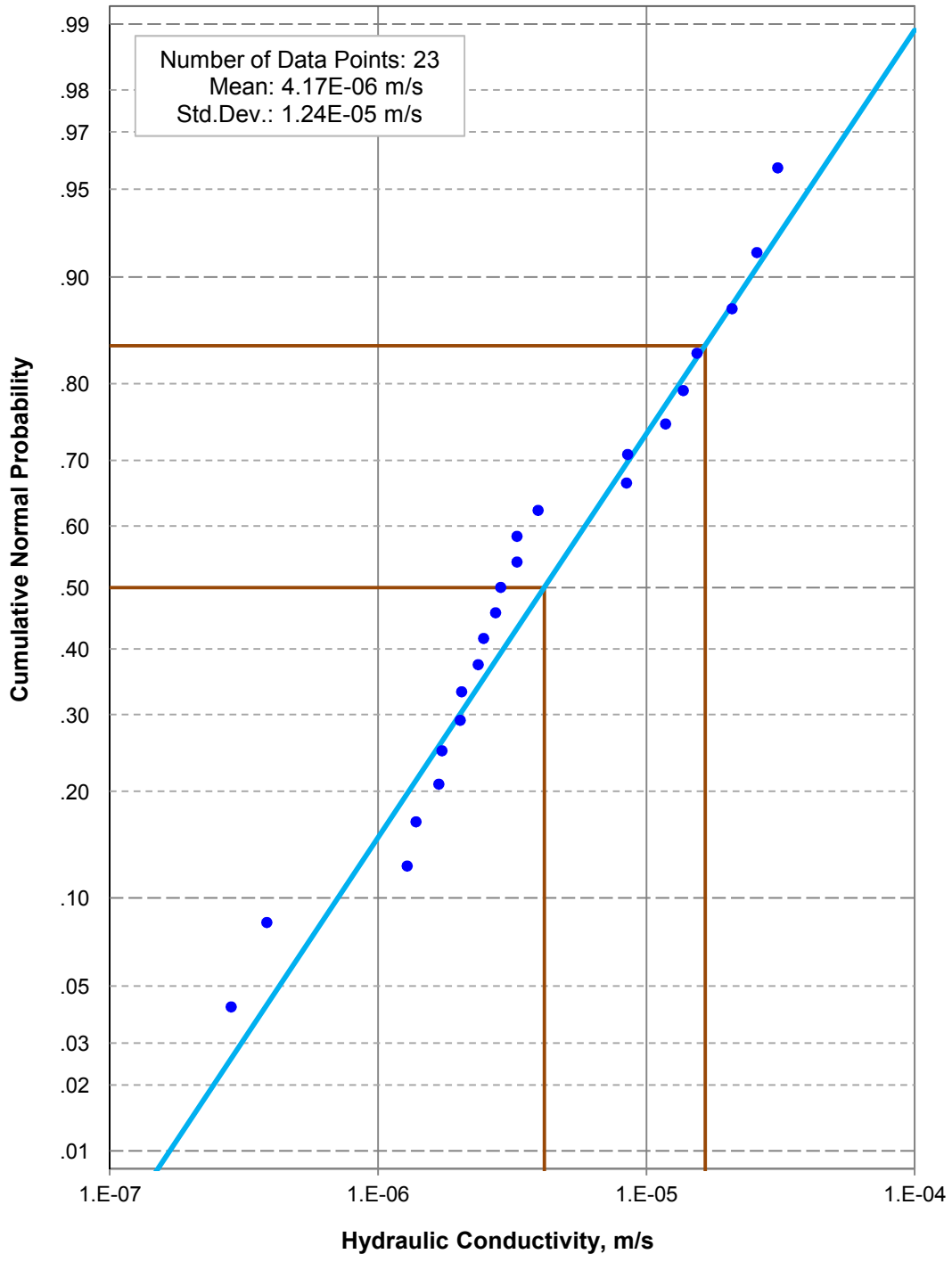

Figure 2.5 Cumulative normal probability plot of the hydraulic conductivities computed from falling head tests on shallow borehole wells.

Project No.	Document Reference
3134	FFC-NL-3134-002
Location	Date
Springpole, ON	February 2021

FFC

Figure 2.6a Locations of GPR profiles along the southeast trail in the area of the proposed Mine Rock & Tailings.	Project No. 3134	Document Reference FFC-NL-3134-002	FFC
	Location Springpole, ON	Date November 2020	

Figure 2.6b Locations of GPR profiles along the northwest trail in the area of the proposed Mine Rock & Tailings.

Project No. 3134	Document Reference FFC-NL-3134-002
Location Springpole, ON	Date November 2020

FFC

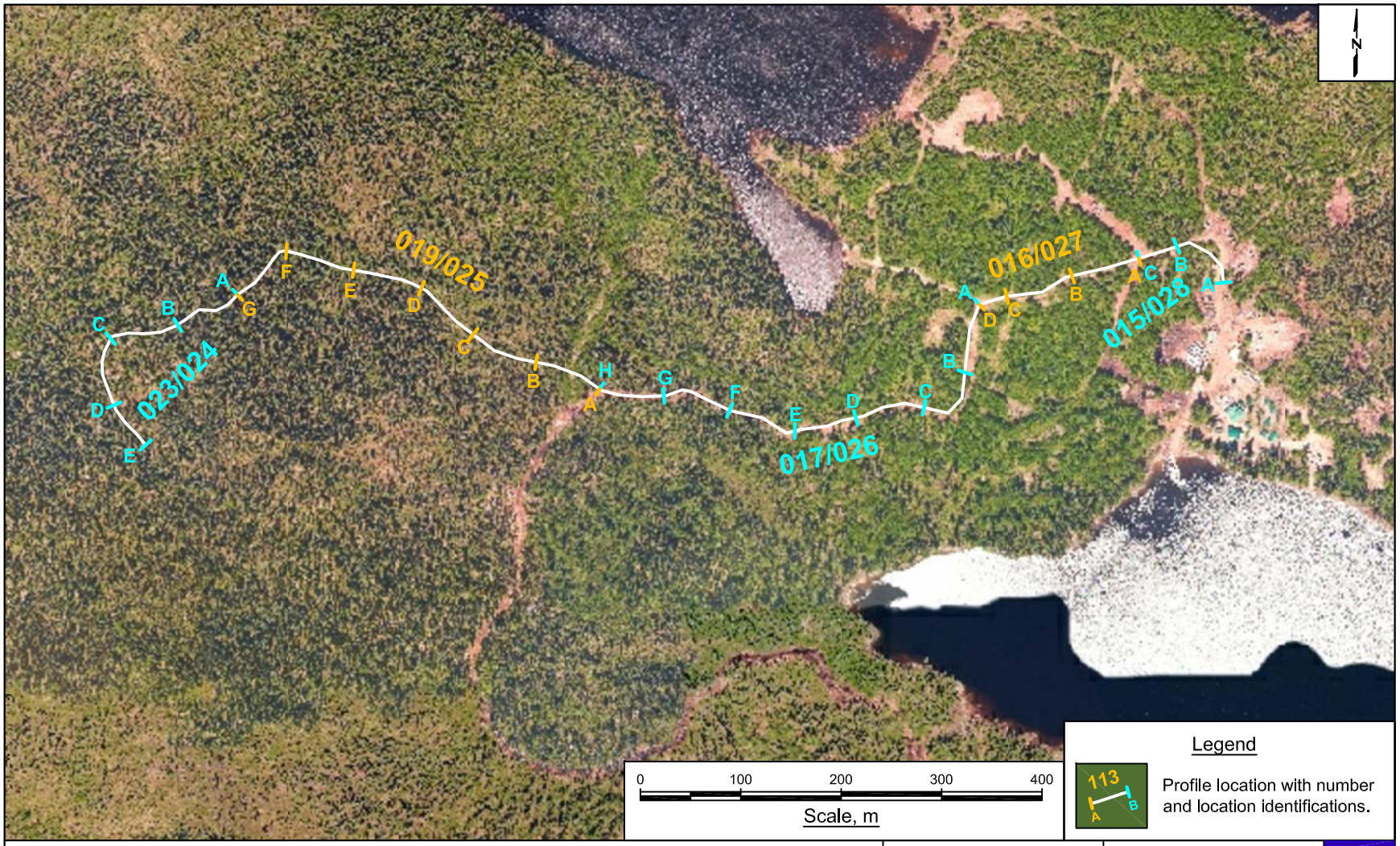

Figure 2.6c Locations of GPR profiles along the existing trail between Birch Lake and Springpole Lake.

Project No. 3134	Document Reference FFC-NL-3134-002
Location Springpole, ON	Date November 2020

FFC

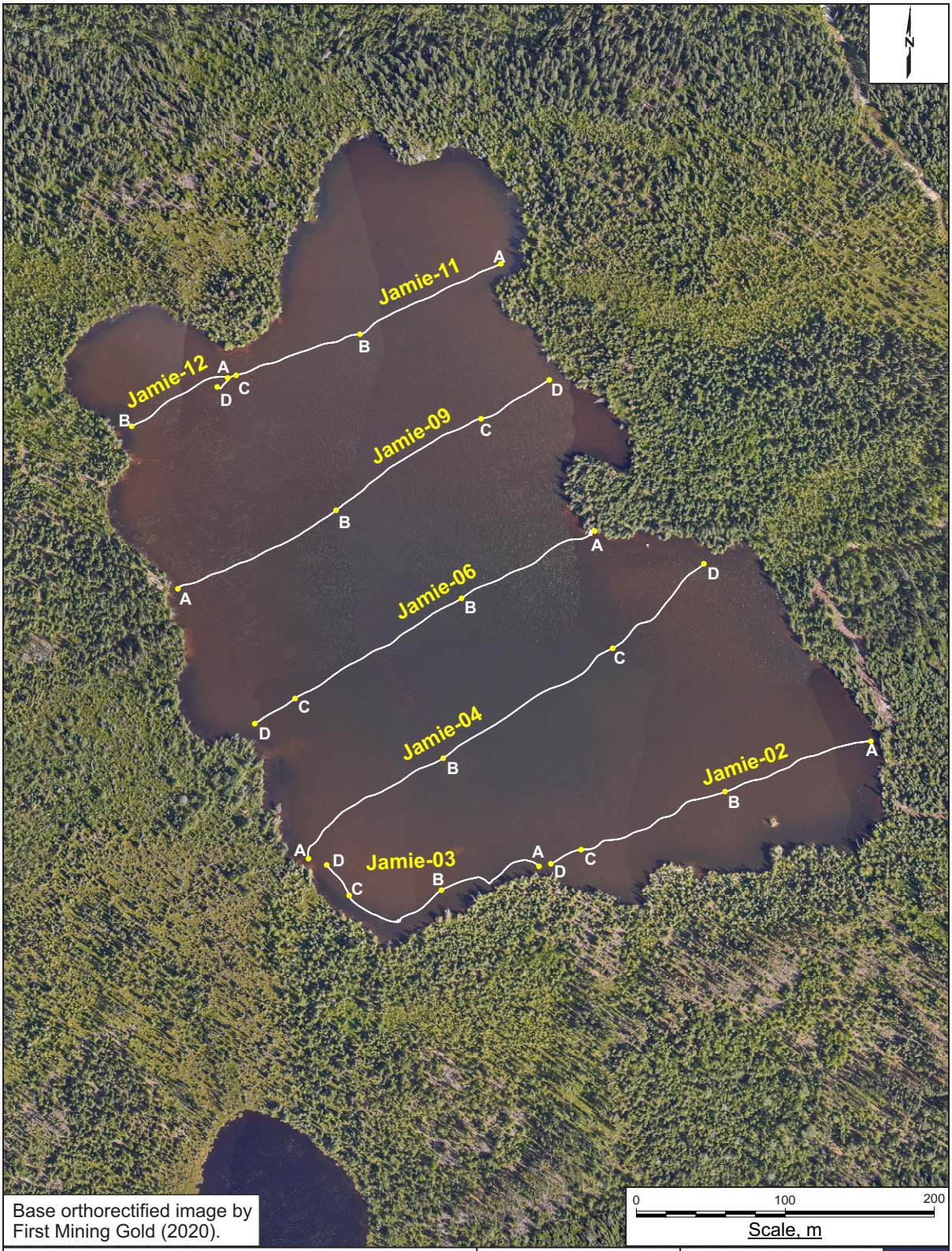

Figure 2.7 Location of the GPR survey conducted on the water (lake) surface at Jamie Lake in August 2020.

Project No.	Document Reference
3134	FFC-NL-3134-002
Location	Date
Springpole, ON	February 2021

FFC

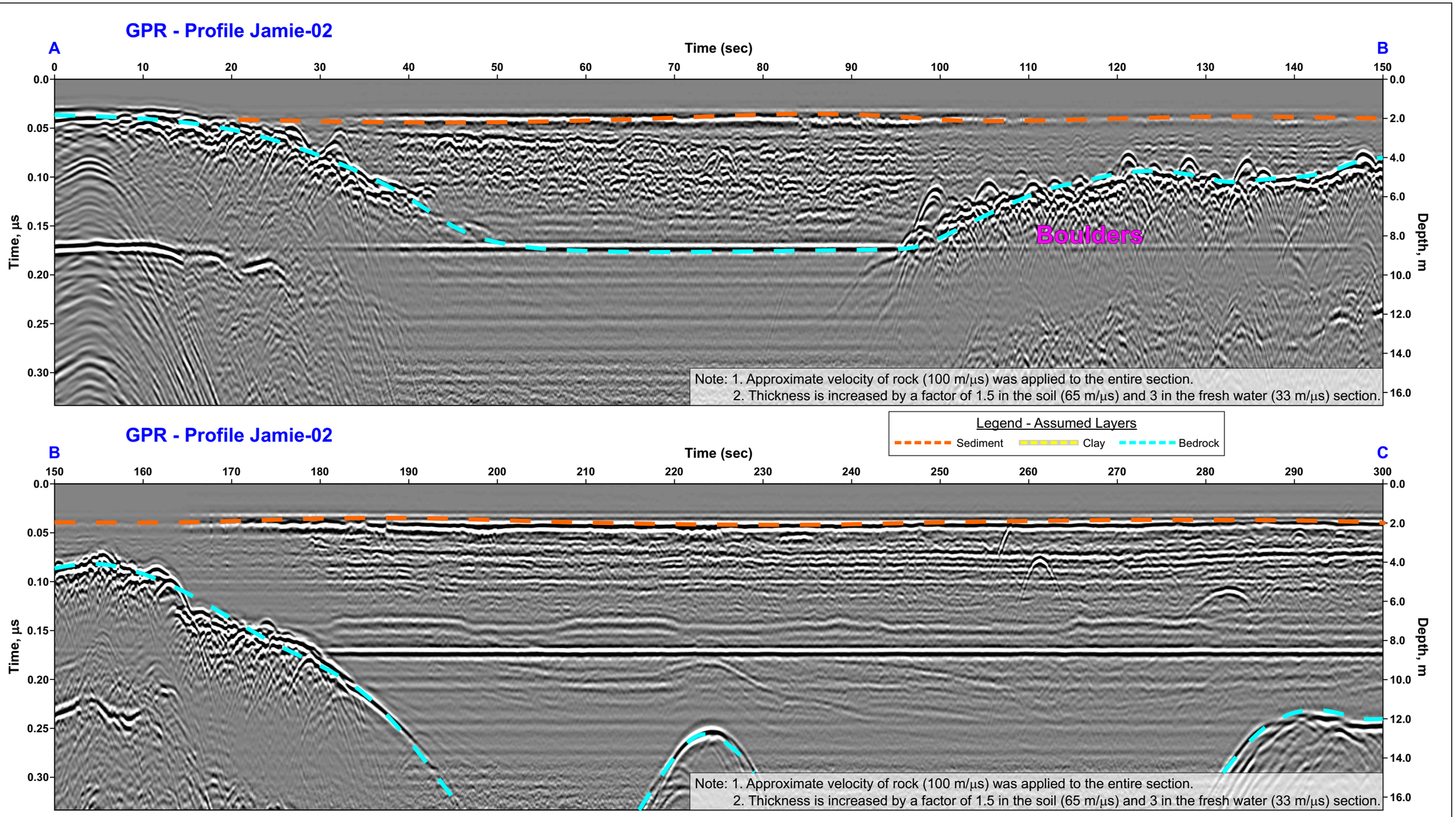

Figure 2.8 Ground penetrating radar survey on water (lake) surface using 170 MHz antenna for Profile Jamie-02 at the Springpole site, ON.

Project No.	Document Reference
3134	FFC-NL-3134-002
Location	Date
Springpole, ON	February 2021

FFC

3.0 FRACTURE GEOMETRY AND MAJOR STRUCTURES

3.1 Introduction

The geology map of the immediate Springpole Lake Project site (**Figure 1.2**) extracted from the First Mining Gold 2016 map compilation, and the Gold Canyon Resources 2005 property wide geology map by L.I. Kovacs and S. Bernales indicates that, based on shoreline outcrops, the main or dominant structural features have a northwest to southeast strike with northeast dips, with a more limited northeast to southwest striking and northwest dipping set of structures. It is assumed that the 2016 map is showing the orientation of small scale structures such as joints or fractures and foliation. West of the proposed main open pit, near the shoreline of Birch Lake, a northwest-southeast trending anticlinal structure was mapped. The 2005 and 2016 maps both show that the shear zones that have been mapped or inferred have a northwest to southeast trend. However, at the immediate southeast side of the Springpole Lake Project site, both geological maps show a major lithological offset that has a northeast to southwest strike.

The bedrock in the immediate project area is primarily mafic and felsic metavolcanic rocks with a small zone of intrusive rocks such as Quartz Porphyry and Feldspar Porphyry on the east side of the main open pit which also extends into the starter pit (Kovacs and Bernales, 2005). A band of clastic sediments is located to the northeast of the immediate project area and it is assumed that those clastic sediments are also metamorphosed to some extent. The permeability of the intact (matrix) metavolcanic and intrusive rocks is generally very low with the overall rock mass permeability being contributed by the discontinuities, such as foliation, joints, fractures, fracture zones and shear zones, in the rock mass. It is the density, lengths, interconnections and orientations of those structures, along with the hydraulic gradients, that control the development of the groundwater flow system and determine the extent to which pit dewatering will impact adjacent areas and the volume and quality of the mine water inflow.

While some core orientation work may have been completed by past workers on this site, there were no records available to show the subsurface fracture patterns. A major focus of the hydrogeology program was to measure the subsurface fracture orientations, determine the fracture densities or spacings, and to identify and describe the intersections of any major structures in boreholes. In 2019, the fracture mapping work consisted of Acoustic Televiewer (AT) surveys in existing exploration boreholes. In 2020, the SGH borehole drilling program provided core to help characterize the fractures and to supplement the AT surveys.

3.2 Acoustic Televiewer Surveys

AT surveys were completed or attempted in 21 inclined boreholes at the Springpole site (**Figure 3.1**) in 2019 (**Appendix D**). **Table 3.1** and **Table 3.2** provide the length and orientation of each borehole and the length of each borehole that was surveyed using the AT tool in 2019 and in 2020. AT logging was suspended in some of the inclined boreholes when large cavities or

borehole washout zones were encountered that would cause the AT probe to drop into the cavity and prevent the AT probe from safely traversing the cavity.

Figure 3.2 shows part of the AT WellCAD log for borehole BL-0035. The AT WellCAD logs for the other boreholes that were surveyed are included in the Fracflow (2020b) factual report. Each AT WellCAD log shows the fracture traces, the computed fracture dip, and the dip direction for each of the fracture traces. Traces that appeared to be welded fractures, foliation grooves, or bit/reamer marks have been identified as well. The apparent width of each of the large open fractures, or mechanical aperture, were also measured and are provided in **Table 3.3** for the 21 AT logs completed in 2019 and in **Table 3.4** for the 11 AT logs that were completed in 2020 (Fracflow, 2020b). The location of each of those 11 boreholes that was mapped in 2020 is shown in **Figure 3.3**.

The tabulated fracture location, orientation and mechanical aperture (or width at the borehole wall) for a selected group of AT logs are presented in Fracflow (2020b). Stereoplots for selected sections of each borehole are included in each AT WellCAD log. Where the bedrock was identified in the original borehole log, the AT log also shows the bedrock units that were cored and the fracture zones or fault/shear zones as evidenced by closely spaced fractures or borehole intervals where the rock is broken, intensely fractured or where core loss is obvious.

3.3 Fracture Orientations

Since single boreholes only intersect part of the fracture system and each borehole will preferentially intersect those fracture planes that are perpendicular or sub-perpendicular to the borehole direction, data from a single borehole does not capture the full range of fracture orientations in the rock mass. In addition, since the normal approach is to display the fracture orientations by plotting the pole or normal to each fracture plane on a stereonet or as a spherical distribution and then contouring the pole densities, the pole contour maps will be dominated by the most frequently intersected fractures especially where the boreholes are long or the borehole lengths vary. While fracture stereonets can be corrected for borehole orientation bias using established equations, during the initial stages of a rock mass investigation, the overall fracture geometry is best assessed by combining fracture data from boreholes that have a range of orientations at each location, if possible. In addition, the AT logs provide data that can be used to weight fractures with widely-spaced intersections along any given borehole, that may be mechanically and/or hydraulically important, to ensure that those fractures do not get underweighted by the density contouring process.

Figure 3.4a shows the individual contour plots for the fractures that were intersected by each of the 21 boreholes that were AT mapped in 2019. **Figures 3.4b** shows the contour plots for the fractures that were intersected in each of the 11 boreholes that were mapped in 2020. The bearing and plunge of each borehole is also shown for each contour plot, along with the number of fracture planes and the dip and dip direction for each major pole cluster.

While the available exploration boreholes in 2019 had orientations that were primarily northeast-southwest, the fractures from the individual boreholes, a number of which had southeast to northwest bearing, that were AT logged in 2020 had a slightly more diverse set of orientations. The 2019 fracture data contour plots of the poles to the fracture planes tended to show one main cluster with a general northwest to southeast strike and a northeast dip, except for the fractures that were intersected by those boreholes that had a northeast bearing. The individual borehole fracture plane pole contour maps for the 2020 boreholes tended to show one strong cluster with an east to west of northwest to south east trend and at least one weaker cluster that has a northeast to southwest trend. In several of the boreholes the sub-horizontal fracture set is well represented.

The 11,753 fractures that were identified in all 21 boreholes in the 2019 AT program were combined in one single contour pole steroplot (**Figure 3.5**). This contour plot confirms that the dominant strike of the discontinuities is approximately northwest to southeast with a northeast dip. The 3,446 fractures or discontinuities (**Figure 3.6**) that were mapped in the HQ boreholes that were drilled in 2020 also had a dominant cluster with a west to northwest strike and a north to northeast dip. The pole plots for those 2020 boreholes also show a weaker cluster with a north to northeast strike.

The average fracture or discontinuity frequency in the boreholes that were AT logged in 2019 ranged from 2.2 to 19 fractures when averaged over a 3 m interval (**Table 3.3**). By comparison, the AT data for the boreholes that were logged in 2020 around the pit perimeter had fracture or discontinuity frequencies that ranged from 0.4 to 2.9 per 3 m interval. The differences in fracture frequency confirms that the dominant fracture set is oriented approximately perpendicular to the 2019 borehole orientations.

3.4 Fracture Widths and Fracture Spacing

The AT logs also provide a direct measure of the mechanical fracture aperture where each fracture intersects the borehole wall. While the mechanical fracture apertures, as opposed to the hydraulic apertures, at the borehole wall are somewhat enlarged by the drilling process, the measured mechanical apertures do provide an indication of how many of the fractures or discontinuities are open and will conduct water. **Figure 3.7** and **Figure 3.8** show the distribution of apertures for two boreholes, BL-0035 and BL-0357, respectively, where most of the fractures that form traces in the borehole wall are not open at the borehole wall. Included at the top of the first column in each histogram is the number of fractures that had zero aperture or no discernible opening or width based on the AT image. In addition, all of the large fractures or structures that had widths greater than 20 mm are shown as the last column in each borehole group and section.

The very large apertures or fracture widths would normally produce high fracture permeability. However, the air-lift test data and the packer test data that were completed in 2019 and 2020 and

presented in this report do not show the expected large increase in fracture permeability that would correlate with the large fracture apertures. Either the fractures are filled with a low to intermediate permeability material or the average fracture spacing is much larger than the average fracture length producing a poorly connected fracture network.

3.5 Fracture Geometry and Major Structures

Major structures are known to exist in the rock mass around the proposed open pit and within the orebody. Other major structures have been either mapped or inferred from basic geological principles or from air photo images and are shown on the site geology map in **Figure 1.2**. However, while the general trend of the major features has been inferred, the actual strike and dip of those features have not been reported.

The core from the SGH boreholes and the vertical borehole that was drilled and tested in 2020 was used to identify zones in each borehole that appear to represent major structures that may have hydraulic significance (**Table 3.5**). The borehole intersections ranged from 0.4 m for zones with well-developed parallel fractures to intensely fractured intersections that measured up to 162 m. It is recognized that borehole intersections are not a measure of the width of any given fracture zone or discontinuity.

Since it is recognized by most workers that the large scale structures mimic the orientation of the small scale structures, it is reasonable to assume that the large scale structures that were intersected by the 2020 boreholes, and by other project boreholes, have a west to northwest strike and dip to the north-northeast. If only the borehole intersections which are intensely fractured and are longer than 10 m are considered, the immediate main open pit rock mass contains a number of large scale features that will produce a strongly elliptical drawdown cone around the pit excavations.

Table 3.1 Specifications of the boreholes logged using acoustic televiewer in 2019 and the logging depths.

Hole ID	Easting	Northing	Distance to Hole Bottom	Azimuth	Dip	Distance to AT Logged
	UTM NAD83-15		(m)	(Degree)	(Degree)	(m btoc[1])
Open Pit Area						
BL-0024	548927.4	5693981.8	252.0	24	-60	243.5
BL-0034	549369.9	5694153.4	614.5	204	-65	499.5
BL-0035	549436.7	5694166.7	611.4	204	-65	495.8
BL-0048	549504.0	5694274.9	286.0	204	-50	276.2
BL-0049	549443.2	5694277.4	228.0	198	-50	220.8
BL-0050	549259.3	5694225.0	374.0	204	-75	371.4
BL-0052	548916.4	5694333.4	462.1	198	-75	455.2
BL-0077	548882.5	5694232.7	322.0	198	-60	307.8
BL-0098	549028.4	5694095.2	282.2	204	-65	278.2
BL-0104	548882.5	5694232.9	307.0	198	-69	302.3
BL-0111	549483.5	5694377.1	496.0	204	-65	485.2
BL-0219	549618.5	5694094.9	155.0	198	-80	144.7
BL-0226	549634.1	5694137.1	94.0	198	-80	91.0
BL-0232	549654.3	5694099.6	124.1	288	-60	117.4
BL-0283	548812.5	5694192.8	87.0	198	-50	32.5
BL-0284	548827.7	5694192.0	84.4	198	-50	82.4
Mine Rock & Tailings Area						
BL-0143	549049.1	5693629.7	764.1	38	-70	483.8
BL-0321	548908.7	5693707.6	228.0	36	-45	223.8
BL-0322	549850.1	5692576.7	386.2	40	-45	73.3
BL-0334	548847.1	5692193.7	324.0	230	-45	100.2
BL-0357	549473.1	5692454.7	200.3	90	-45	65.3

Note [1] btoc: below top of casing.

Table 3.2 Summary of acoustic televiewer survey data for the 11 boreholes located around the proposed Open Pit for the SGH2020 program.

Hole ID	Easting	Northing	Distance to Hole Bottom	Azimuth	Dip	Distance to AT Logged
	UTM NAD83-15		(m)	(Degree)	(Degree)	(m btoc[1])
Open Pit Area - Pit Slope Stability						
SGH20-001	549339.3	5693014.6	400.1	90	-55	232.3
SGH20-002	548918.2	5693693.4	400.0	137	-50	383.3
SGH20-004	548811.9	5694074.3	293.0	169	-50	285.2
SGH20-005	549018.5	5694323.6	401.0	121	-53	399.8
SGH20-006	549959.3	5693537.7	440.0	190	-52	439
SGH20-007	549578.5	5693987.5	401.0	147	-52	399.7
SGH20-008	549327.5	5694166.8	413.0	125	-52	412.1
SGH20-009	549217.4	5693348.8	392.0	125	-52	74.9
Coffer Dam Area						
SGH20-003	549813.2	5692526.8	410.0	96	-50	104.5
SGH20-010	550894.1	5693411.8	401.0	189	-50	191.2
Test Well						
SPW20-001	549026.0	5694165.9	401.0	--	-90	356

Note [1] btoc: below top of casing.

Table 3.3 Specifications of the acoustic televiewer logging and summary of fracture data for the selected 21 existing boreholes.

Hole ID	Distance to Logging (m btoc[1])		Total Logging Length (m btoc[1])	Total Number of Fracture	Open Fracture (%)		Fracture Frequency per 3 m
	Start	End			0 - 10 mm	> 10 mm	
Open Pit Area							
BL-0024	6.1	243.5	237.4	923	25.4	0.7	11.7
BL-0034	9.8	499.5	489.7	1078	19.4	1.4	6.6
BL-0035	8.6	495.8	487.2	501	22.5	3.8	3.1
BL-0048	6.1	276.2	270.1	196	16.3	0.5	2.2
BL-0049	4.1	220.8	216.7	347	21.9	0.6	4.8
BL-0050	19.6	371.4	351.8	267	13.9	0.7	2.3
BL-0052	9.2	455.2	446.0	592	10.1	1	4.0
BL-0077	6.6	307.8	301.2	877	7	0.3	8.7
BL-0098	7.8	278.2	270.4	915	13.7	0.5	10.2
BL-0104	7.3	302.3	295.1	339	16.8	0.9	3.4
BL-0111	5.5	485.2	479.7	1796	7.4	0.7	11.2
BL-0219	8.3	144.7	136.4	569	13.7	0.9	12.5
BL-0226	9.4	91.0	81.6	398	5.8	0	14.6
BL-0232	7.9	117.4	109.5	483	19.3	0.8	13.2
BL-0283	5.4	32.5	27.1	45	35.6	4.4	5.0
BL-0284	6.7	82.4	75.7	362	16.8	0.6	14.3
Mine Rock & Tailings Area							
BL-0143	7.6	483.8	476.2	922	8.4	0.1	5.8
BL-0321	9.6	223.8	214.2	199	25.1	0	2.8
BL-0322	8.3	73.3	65.0	202	20.3	2.5	9.3
BL-0334	5.8	100.2	94.4	597	21.3	2.2	19.0
BL-0357	4.8	65.3	60.5	145	33.8	0.7	7.2

Note [1] btoc: below top of casing.

Table 3.4 Specifications of the acoustic televiewer logging and summary of fracture data of 11 boreholes for the SGH2020 program.

Hole ID	Distance to Logging (m btoc[1])		Total Logging Length (m btoc[1])	Total Number of Fracture	Open Fracture (%)		Fracture Frequency per 3 m
	Start	End			0 - 10 mm	> 10 mm	
Open Pit Area - Pit Slope Stability							
SGH20-001	14.7	232.3	217.6	248	14.5	1.2	1.1
SGH20-002	11.6	383.3	371.7	404	14.9	1.7	1.1
SGH20-004	18.8	285.2	266.4	199	10.6	1.5	0.7
SGH20-005	14.4	399.8	385.4	264	10.2	0.8	0.7
SGH20-006	13.0	439.0	426.0	840	10.2	1.1	2.0
SGH20-007	14.0	399.7	385.7	313	17.8	1.0	0.8
SGH20-008	14.0	412.1	398.1	178	12.9	1.7	0.4
SGH20-009	15.0	74.9	59.9	105	28.5	2.9	1.8
Coffer Dam Area							
SGH20-003	14.6	104.5	89.9	224	19.6	1.8	2.5
SGH20-010	18.0	191.2	173.2	506	14.5	1.6	2.9
Test Well							
SPW20-001	11.5	356.0	344.6	210	15.7	3.3	0.6

Note [1] btoc: below top of casing.

Table 3.5 Major structures and fracture/fault/breccias/shear intersections for the 11 boreholes around the Open Pit for slope stability (Page 1 of 3).

Top of Structure (m)	Bottom of Structure (m)	Length of Intersection (m)	Description of Structure
SGH20-001			
227.3	233.0	5.7	Highly broken core with vuggy surface
233.0	235.4	2.4	Highly fractured zone
235.4	238.5	3.1	Intensely fractured zone with fault gauge/breccia
238.5	266.9	28.4	Intensely fractured zone
266.9	272.0	5.1	Highly fractured zone
272.0	300.3	28.3	Intensely fractured zone
300.3	305.3	5.0	Highly fractured zone
305.3	328.1	22.8	Intensely fractured zone
328.1	357.1	29.0	Highly fractured zone
SGH20-002			
343.5	345.3	1.8	Highly fractured zone
SGH20-003			
41.0	51.5	10.5	Highly fractured zone
123.0	158.0	35.0	Highly fractured broken zone
164.0	189.5	25.5	Highly fractured broken zone
200.0	236.0	36.0	Intensely fractured broken zone
264.5	264.9	0.4	Intensely fractured cores
303.0	303.2	0.2	Intensely fractured cores
319.7	320.0	0.3	Highly fractured cores
352.5	353.0	0.5	Intensely fractured cores
366.0	371.0	5.0	Highly fractured zone
377.0	385.7	8.7	Highly fractured zone
390.6	399.6	9.0	Intensely fractured zone
399.6	410.0	10.4	Highly fractured zone
SGH20-004			
15.5	16.5	1.0	Subparallel fractures to the core axis
24.0	27.0	3.0	Highly fractured broken cores
28.7	32.0	3.3	Highly fractured cores
271.0	275.4	4.4	Subparallel fractures to the core axis
SGH20-005			
45.0	46.0	1.0	Subparallel fractures to the core axis
147.9	148.7	0.8	Highly fractured cores
330.7	332.0	1.3	Highly fractured cores

Table 3.5 Major structures and fracture/fault/breccias/shear intersections for the 11 boreholes around the Open Pit for slope stability (Page 2 of 3).

Top of Structure (m)	Bottom of Structure (m)	Length of Intersection (m)	Description of Structure
SGH20-006			
32.0	37.0	5.0	Highly fractured cores
61.0	61.4	0.4	Subparallel fractures to the core axis
92.6	102.4	9.8	Highly fractured broken cores
143.5	144.1	0.6	Highly fractured broken cores
160.3	161.1	0.8	Highly fractured broken cores
178.3	182.7	4.4	Highly fractured cores
236.5	239.0	2.5	Highly fractured cores
254.7	265.4	10.7	Intensely fractured zone with broken cores
283.5	285.1	1.6	Highly fractured cores
288.5	290.0	1.5	Highly fractured broken cores
292.3	299.8	7.5	Highly fractured vuggy cores
307.8	308.2	0.4	Subparallel fractures to the core axis
328.0	330.7	2.7	Intensely fractured zone with broken cores Subparallel fractures to the core axis
341.8	343.8	2.0	Highly fractured vuggy cores
347.0	366.0	19.0	Highly fractured, vuggy, broken cores
SGH20-007			
53.5	55.8	2.3	Highly fractured broken cores
90.7	91.4	0.7	Highly fractured broken cores
300.5	301.5	1.0	Subparallel fractures to the core axis
379.0	379.4	0.4	Subparallel fractures to the core axis
SGH20-008			
129.1	129.5	0.4	Subparallel fractures to the core axis
339.5	340.8	1.3	Highly fractured broken cores
SGH20-009			
38.4	40.7	2.3	Highly fractured cores
73.3	73.9	0.5	Fault gauge/breccia
106.8	110.0	3.2	Highly fracture cores
115.4	160.0	44.6	Highly fractured cores
150.5	230.0	79.5	Highly fractured zone
230.0	392.0	162.0	Intensely fractured zone

Table 3.5 Major structures and fracture/fault/breccias/shear intersections for the 11 boreholes around the Open Pit for slope stability (Page 3 of 3).

Top of Structure (m)	Bottom of Structure (m)	Length of Intersection (m)	Description of Structure
SGH20-010			
55.8	56.6	0.8	Highly fractured cores
65.0	83.0	18.0	Highly fractured broken cores
163.0	164.0	1.0	Highly fractured broken cores
178.2	179.7	1.5	Highly fractured broken cores
278.5	281.0	2.5	Highly fractured broken cores
281.5	287.5	6.0	Highly fractured broken cores
293.7	295.0	1.3	Highly fractured broken cores
SPW20-001			
355.5	362.3	6.8	Highly fractured broken cores
366.4	370.0	3.6	Highly fractured broken cores